Fast mapping of absorbing defects in optical materials by full-field photothermal reflectance microscopy

Woo June Choi, Seon Young Ryu, Jun Ki Kim, Jae Young Kim, Dong Uk Kim, and Ki Soo Chang*

Center for Analytical Instrumentation Development, Korea Basic Science Institute (KBSI), 169-148 Gwahak-ro, Yuseong-gu, Daejeon 305-806, South Korea

**Corresponding author: ksc@kbsi.re.kr*

Received September 3, 2013; revised October 21, 2013; accepted October 23, 2013; posted October 25, 2013 (Doc. ID 196943); published November 15, 2013

We report a technique for rapidly mapping absorbing defects in optical materials, which act as laser-induced damage precursors, based on full-field photothermal reflectance microscopy. An intensity-modulated pump beam heats absorbing defects in the optical sample, creating localized, modulated refractive-index variations around the defects. A probe beam then illuminates the defect sites, and the measured amplitude of the reflectance variation is used to map the distribution of defects in the medium. Measurements show that this method offers a faster defect mapping speed of about 0.03 mm^2 per minute and a detectivity of a few tens of nanometers comparable to that of conventional scanning photothermal deflection microscopy.

OCIS codes: (110.0180) Microscopy; (140.3330) Laser damage; (350.5340) Photothermal effects.
http://dx.doi.org/10.1364/OL.38.004907

In optical coating manufacturing, it is well known that micrometer- and nanometer-sized defects (such as cracks, impurities, and contaminants) are major precursors of laser-induced damage in dielectric optical components [1–3]. In high-power laser applications, these damage precursors induce highly localized thermal stress in the homogeneous optical material under laser illumination, which lowers the laser-induced damage threshold (LIDT), leading to material breakdown. Hence, there have been demands for accurate location of the defects to predict the potential laser damage site and secure high-quality optical performance of the optical materials. Photothermal deflection microscopy has become a promising tool to meet such demands [4–10]. The principle behind this technique is that, as an intensity-modulated pump beam gets absorbed by absorbing defects in the medium, the absorbed energy is released to surroundings of the defects as heat, forming highly localized thermal deformations, a refractive-index (RI) gradient around the absorber (thermal lens), and a bump in the surface of the medium because of thermal expansion. The presence of defects is identified by measuring the slight deflection of a probe beam caused by these deformed spots [7–10]. With metal-nanoparticle-embedded optical materials as a test sample, photothermal deflection microscopy was able to offer enhanced contrast in defect identification with a high detectivity of a few tens of nanometers [10].

Although photothermal deflection microscopy is a powerful technique for detecting submicrometer defects with high spatial resolution and detectivity, the slow image acquisition speed (several hundreds of μm^2 – 1 mm^2 per hour depending on the required detectivity [7]), due to the time-consuming point scanning for the reconstruction of the defect map, prevents rapid inspection of a large area of the optical material being characterized. High-speed photothermal deflection imaging of defects has been proposed using a multipixel image sensor and an optical lock-in technique [11]. However, such detection was limited to the highly absorptive defects or relatively large defects (hundreds of micrometers in size) due to the high background noise in the photothermal image. In this Letter, we propose a new full-field photothermal imaging technique utilizing charge-coupled device (CCD)-based thermoreflectance microscopy (TRM) for fast and high-contrast mapping of the micrometer- and nanometer-sized absorbing defects inside the optical material.

TRM is a well-known optical technique for noncontact thermal imaging of activated microelectronic devices and integrated circuits [12–15]. To obtain a thermal image, it measures minute reflectivity changes ($\sim 10^{-3}$) of the sample in response to variation of its surface temperature [15]. This principle can be applied to photothermal imaging to detect local defects inside the optical structure inasmuch as the reflectivity of the probe beam is varied by the temperature-dependent thermal lens around the defects, which absorb the pump beam. The use of a CCD in photothermal reflectance imaging, which eliminates the need for the time-consuming point scan, enables a full-field mapping of defects in parallel, and hence significantly reduces the inspection time for the optical materials.

The experimental setup is shown in Fig. 1. The experiment was performed with two light sources: a diode laser (FreeBeam 808, RGBLaseLLC) at $\lambda = 808$ nm (pump beam) for photothermal excitation of defects and a red light-emitting diode (LED) (MCEP-CR8, Moritex Corp.) at $\lambda = 636$ nm (probe beam) for the thermoreflectance measurement of the photothermally excited defects. The intensity of the pump beam was modulated at a frequency of 1 Hz. The pump beam was expanded to a $1/e^2$ diameter of 7.0 mm with a Gaussian intensity distribution by a large beam collimator and then used to vertically irradiate the sample through the bottom surface. The output power of the pump beam was varied between 0.5 and 8.0 W depending on the degree of optical absorption by the defects in the optical materials to be mapped. The red probe beam was focused into the top surface of the sample through a long working distance

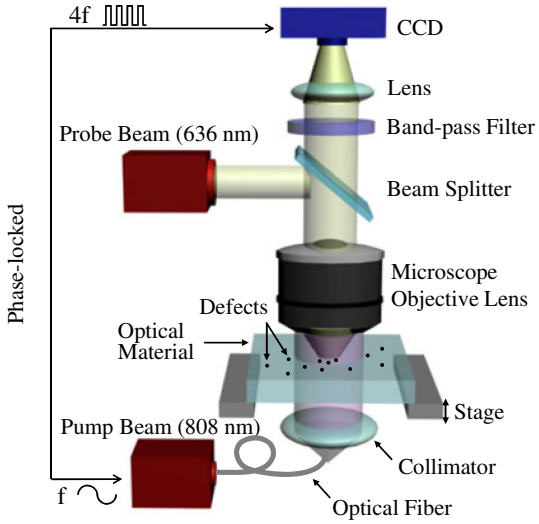

Fig. 1. Schematic representation of photothermal reflectance microscopy.

(W.D. = 13 mm) microscope objective (M Plan Apo, 50×, numerical aperture (N.A.) = 0.55, Mitutoyo), resulting in an incident optical power on the sample of 17 mW. The small illuminated sample area of the probe beam (0.6 mm^2) was centered on the large irradiated sample area of the pump beam (38.5 mm^2), which ensured uniform pump beam irradiation within the probing area of the sample. Under the irradiation of the intensity-modulated pump beam, the absorbing defects yielded a time-varying localized RI around each of the defects (thermal lenses). Parts of the probe beam were then reflected from the localized thermal lenses in the probing path, resulting in a time-varying reflected beam that was collected by the objective lens and delivered to a visible CCD camera (pco. 1600, 1600 × 1200 pixels, 14 bits, PCO AG) through a band-pass optical filter (center wavelength = 636 nm), which rejected the pump beam. To measure the small amplitude (on the order of 10^{-3} to 10^{-5}) of the thermoreflectance signal modulation at the defect site, a well-known four-bucket technique was used for the homodyne optical lock-in measurement [15]. For this measurement, the CCD camera was synchronized (phase-locked) with the intensity modulation of the pump beam and triggered at four times (4 Hz) the modulation frequency of the pump beam (1 Hz) to capture four CCD frames per the modulation period of the pump beam (1 s). Cumulative averaging over the thermoreflectance measurement results was also used to improve the signal sensitivity [14,15].

To verify the practicability of using photothermal reflectance microscopy for the mapping of absorbing defects in optical materials, a 100-μm-thick single polydimethylsiloxane (PDMS, RI = 1.43 at 810 nm) layer containing 5.3-μm-diameter polystyrene beads (RI = 1.58 at 810 nm) was prepared to simulate a defective optical material and was imaged with the system. Relatively large microbeads exceeding the optical diffraction limit (543 nm) were used to compare the photothermal reflectance image with an optical image of the same microbeads. The PDMS layer is highly transparent at the visible and near-infrared (NIR) wavelengths [16]. The focal

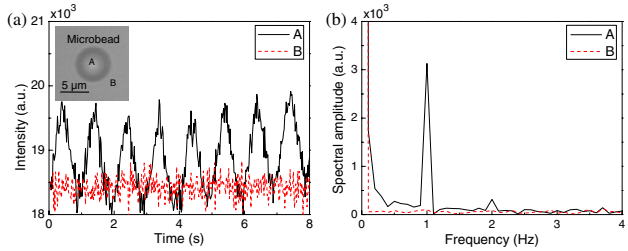

Fig. 2. (a) Plots of reflected intensity waveforms at two different pixel locations, one (A) on the single microbead and the other (B) in the bead-free region in the PDMS mixture under irradiation by the intensity-modulated (1 Hz) pump beam. The positions of the respective pixels are indicated by A and B in the inset. (b) Frequency spectra of the corresponding waveforms in (a).

plane of the probe beam was positioned about 50 μm below the top surface of the sample. The total output power of the pump beam was 7 W with a Gaussian intensity distribution ($1/e^2$ diameter = 7.0 mm), corresponding to an average power density of 45 W/cm^2 for the small probing area of 0.6 mm^2 centered on the large pumping area of 38.5 mm^2. Prior to mapping of the defects, photothermal reflectance phenomena at the defect site were identified. Under the irradiation of the intensity-modulated pump beam (1 Hz), the reflected probe beam distribution from the sample was repeatedly captured by the CCD camera at a frame rate of 50 Hz. Figure 2(a) shows the time-varying reflected intensity signals of the probe beam taken at two different pixels, one corresponding to a location in a single microbead and the other corresponding to a location in a bead-free region (where these locations are indicated as A and B in the inset, respectively) with the recorded 400 CCD frames. In Fig. 2(a), we can see that the signal from A periodically oscillates with large amplitude as compared to the signal from B, the fluctuation of which seems like noise. This difference is apparent in the Fourier domain [as shown in Fig. 2(b)], where a strong spectral peak at 1 Hz is observed in the signal from A, whereas no spectral peaks appear in the signal from B. This means that the thermoreflectance due to the photothermal effect caused by the pump beam intensity modulation at 1 Hz occurs only in the microbead.

Photothermal reflectance imaging was performed with the same sample as in the previous measurement. Figure 3(a) shows an optical microscope image of the individual polystyrene microbeads dispersed in the PDMS layer. In the photothermal reflectance image [Fig. 3(b)],

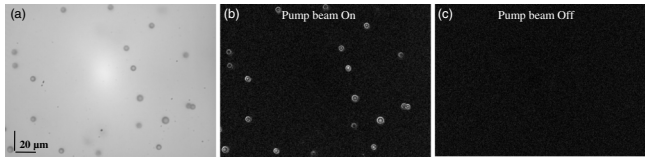

Fig. 3. (a) Optical microscope image at 50 μm below the surface of the 100-μm-thick single PDMS layer containing sparsely dispersed 5.3-μm-diameter polystyrene microbeads. (b), (c) Photothermal reflectance images of the sample when the pump beam is on and off, respectively. The image area is 200 μm(X) × 148 μm(Y).

when the pump laser is on, the thermoreflectance signals appear at the same location as the microbeads in Fig. 3(a) with no signals from the background of the sample, which means that the thermoreflectance signals arise only from the absorbing particles (microbeads). When the pump laser is off, the thermoreflectance signals in the photothermal reflectance image disappear [Fig. 3(c)] due to the absence of the thermal excitation of the particles. These results indicate that the proposed photothermal reflectance imaging method is able to precisely locate the micrometer-sized absorbing defects in the optical medium.

In order to demonstrate the ability of photothermal reflectance microscopy to detect nanometer-sized absorbing defects below the diffraction limit, we realized the mapping of gold nanorods, which are sparsely dispersed in a 50 μm-thick-PDMS layer. Bare gold nanorods (GNRs) (width = 25 nm, length = 102 nm, and aspectratio = 4.1, Nanopartz Inc.) were chosen as well-characterized metallic nanoinclusions due to their strong absorbance in the NIR wavelengths [17]. Photothermal excitation was applied to the GNRs to transform the invisible nanometer-sized GNRs by far-field optics to visible-scale thermal lenses of the PDMS around the GNRs by heating with an intensity-modulated pump beam. The pump beam had an output power of 0.5 W, corresponding to an average power density of 3.3 W/cm^2 in the probing area. The average power density of the pump beam was small and similar to that of the probe beam. However, photothermal excitation of the GNRs is induced by the pump beam only because the absorbance of the GNRs at the pump beam wavelength is more than 10 times larger than that at the probe beam wavelength, which is negligible [17]. Figure 4 represents the photothermal reflectance imaging results at 10 μm below the surface of the sample. In Figs. 4(a) and 4(b), the areas of the images were cropped to 44 μm(X) × 44 μm(Y) from the entire imaged area of 200 μm(X) × 148 μm(Y) for better visualization of the photothermally excited GNRs. An optical microscope image [Fig. 4(a)] shows that the GNRs were not visible because the size of the GNRs is much smaller than the diffraction-limited optical resolution of the system. In the photothermal reflectance image [Fig. 4(b)], however, high-contrast signals arising from the sites of absorbing GNRs were clearly seen. To improve the thermoreflectance sensitivity, 50 thermoreflectance images were accumulated and averaged. This number for averaging was experimentally chosen when the presence of defects in the material was well-identified by its appearance. The resulting measurement time was 50 s, and the mapping speed was ~0.03 mm^2 per minute. There are two dust particles on the PDMS surface visible in the optical microscope image [Fig. 4(a)], but they are not visible in photothermal reflectance image [Fig. 4(b)]. This can be attributed to the dust particles on the surface not being photothermally activated, and thus they were eliminated as DC components during the lock-in process. The signal-to-noise ratio (SNR) of the signal from one location [indicated by the white box in Fig. 4(b)] was measured to be 4.66, as shown in Fig. 4(c), which is comparable to the measured SNR with photothermal deflection microscopy [10]. A histogram [Fig. 4(d)] of the SNRs from 118 individual, well-separated spots from the whole imaged area (200 μm(X) × 148 μm(Y)) shows a quite monomodal distribution, confirming that the signals were derived from the individual GNRs [18].

In our experiment, the photothermal reflectance signals stood out from the background noise only for the defects around the focal plane of the probe beam. This enables the resolution of the defects at different depths in the medium. To evaluate the depth resolution, we imaged the GNRs in the sample of Fig. 4 by shifting the sample in the axial (Z) direction with a step size of 0.14 μm using the linear sample stage. From the obtained 125 photothermal reflectance images at different depths of the sample, photothermal reflectance signals from a single GNR in the images were picked and plotted. Figure 5 shows an axial (Z) profile of the photothermal reflectance signals against the relative displacements of the sample, where it is shown to be fitted well by a Gaussian function. The full width at half-maximum (FWHM) of the curve fit, which represents the depth resolution, was measured to be ~4.42 μm. The depth resolution is related

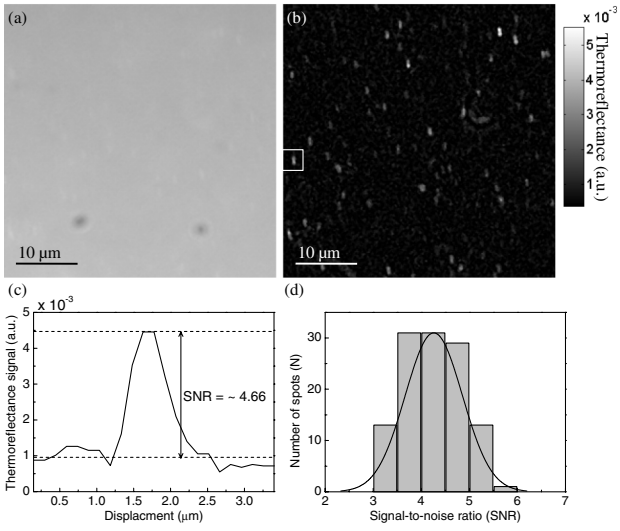

Fig. 4. (a) Optical microscope image (44 μm(X) × 44 μm(Y)) of the 50-μm-thick PDMS layer containing gold nanorods (25 nm(width) × 102 nm(length) with an aspect ratio of 4.1). (b) Photothermal reflectance image of the sample. (c) Spatial profile of the thermoreflectance signal from the location marked by the white box in (b). (d) SNR histogram of 118 detected spots.

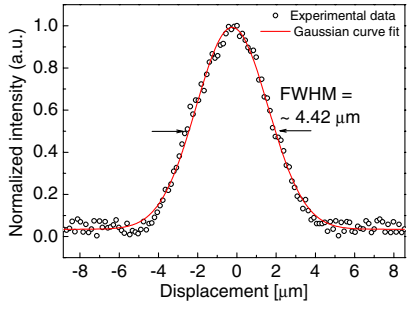

Fig. 5. Measured axial (Z) profile of the photothermal reflectance signals of a single GNR against the relative diplacement of the sample.

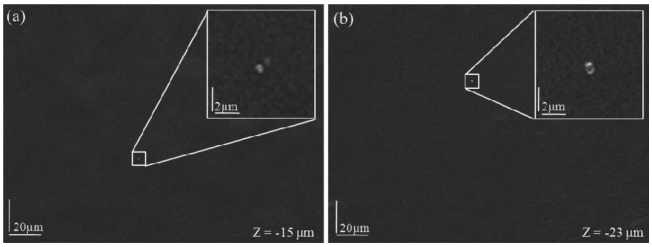

Fig. 6. Photothermal reflectance images (a), (b) obtained with a 80-μm-thick bare PDMS layer at depths of 15 and 23 μm below the surface, respectively. Submicrometer spots are clearly seen in each image, representing the absorbing defects. The average power density of the pump beam was set to 52 W/cm^2 for both measurements. The image (200 μm(X) × 148 μm(Y)) was obtained in 50 s by computing the cumulative average over 50 images.

to the Rayleigh length (i.e., depth of focus) of the objective lens. Therefore, higher resolution can be expected with a shorter Rayleigh length of the objective lens.

To demonstrate defect mapping in the optical material, photothermal reflectance images were obtained for the 80-μm-thick bare PDMS layer containing natural defects. Figures 6(a) and 6(b) represent photothermal reflectance images of the sample at depths of 15 and 23 μm below the surface, respectively. From each image, we found spots (<1 μm in diameter) that stem from local defects, the locations of which are apparent (see the enlarged views in each figure). This demonstration shows that the proposed photothermal reflectance microscopy is capable of mapping the submicrometer absorbing defects located at different depths in bulk optical materials.

In summary, we have demonstrated a new full-field photothermal reflectance microscopy for fast mapping of the absorbing defects inside optical materials, which are responsible for laser-induced damage initiation. In comparison with the previous scanning photothermal deflection microscopy techniques, the proposed system shows much faster defect mapping speed (~0.03 mm^2 per minute), comparable detection sensitivity (a few tens of nanometers), and depth-resolved detection ability (depth resolution of ~4.4 μm). Although this work was an initial demonstration of the feasibility of this system, we believe that such a photothermal reflectance microscopy is a promising candidate for high-speed quality inspection in the manufacturing of optical components for high-power laser applications.

This work was partially supported by a KBSI grant (D33200) and an SMBA grant (S2060032).

References

1. N. Bloembergen, Appl. Opt. **12**, 661 (1973).
2. J.-Y. Natoli, L. Gallais, H. Akhouayri, and C. Amra, Appl. Opt. **41**, 3156 (2002).
3. S. G. Demos, P. DeMange, R. A. Negres, and M. D. Feit, Opt. Express **18**, 13788 (2010).
4. M. Commandré and P. Roche, Appl. Opt. **35**, 5021 (1996).
5. Z. L. Wu, M. Thomsen, P. K. Kuo, Y. Lu, C. Stolz, and M. Kozlowski, Opt. Eng. **36**, 251 (1997).
6. R. Chow, J. R. Taylor, and Z. L. Wu, Appl. Opt. **39**, 650 (2000).
7. A. Gatto and M. Commandré, Appl. Opt. **41**, 225 (2002).
8. A. During, M. Commandré, C. Fossati, B. Bertussi, J.-Y. Natoli, J.-L. Rullier, H. Bercegol, and P. Bouchut, Opt. Express **11**, 2497 (2003).
9. A. During, C. Fossati, and M. Commandré, Opt. Commun. **230**, 279 (2004).
10. B. Bertussi, J.-Y. Natoli, and M. Commandré, Appl. Opt. **45**, 1410 (2006).
11. C. J. Stolz, D. J. Chinn, R. D. Huber, C. L. Weinzapfel, and Z. L. Wu, Proc. SPIE **5273**, 141 (2004).
12. J. Christofferson and A. Shakouri, Rev. Sci. Instrum. **76**, 24903 (2005).
13. G. Tessier, M.-L. Polignano, S. Pavageau, C. Filloy, D. Fournier, F. Cerutti, and I. Mica, J. Phys. D **39**, 4159 (2006).
14. P. M. Mayer, D. Lüerßen, R. J. Ram, and J. A. Hudgings, J. Opt. Soc. Am. A **24**, 1156 (2007).
15. M. Farzaneh, K. Maize, D. Lüerßen, J. A. Summers, P. M. Mayer, P. E. Raad, K. P. Pipe, A. Shakouri, R. J. Ram, and J. A. Hudgings, J. Phys. D **42**, 143001 (2009).
16. D. K. Cai, A. Neyer, R. Kuckuk, and H. M. Heise, Opt. Mater. **30**, 1157 (2008).
17. X. Huang, P. K. Jain, I. H. El-Sayed, and M. A. El-Sayed, Lasers Med. Sci. **23**, 217 (2008).
18. D. Boyer, P. Tamarat, A. Maali, B. Lounis, and M. Orrit, Science **297**, 1160 (2002).